Large enhancement of the thermoelectric power factor in disordered materials through resonant scattering

S. Thébaud,* Ch. Adessi, and G. Bouzerar

Université Claude Bernard Lyon 1, Centre National de la Recherche Scientifique, Institut Lumière Matière, F-69622 Lyon, France

(Received 25 February 2019; revised manuscript received 19 April 2019; published 6 June 2019)

In the search for more efficient thermoelectric materials, scientists have placed high hopes in the possibility of enhancing the power factor using resonant states. In this paper, we investigate theoretically the effects of randomly distributed resonant impurities on the power factor. Using the Chebyshev polynomial Green's-function method, we compute the electron transport properties for very large systems ($\sim 10^7$ atoms) with an exact treatment of disorder. The introduction of resonant defects can lead to a large enhancement of the power factor together with a sign inversion in the Seebeck coefficient. This boost depends crucially on the position of the resonant peak, and on the interplay between elastic impurity scattering and inelastic processes. Strong electron-phonon and electron-electron scatterings are found detrimental. Finally, the robustness of our results is examined in the case of anisotropic orbitals and two-dimensional confinement. Our findings are promising for the prospect of thermoelectric power generation.

DOI: 10.1103/PhysRevB.99.245203

I. RESONANT STATES IN THERMOELECTRIC MATERIALS

Over the past decades, the increasingly pressing need for clean energy sources and the realization that a huge proportion of the energy used worldwide is wasted in heat [1] have prompted great interest in the prospect of developing efficient thermoelectric generation modules [2–5]. The currently available devices, mainly based on $(Bi,Sb)_2Te_3$, PbTe or Si-Ge alloys, are not efficient enough to be used industrially on a large scale [6]. The efficiency of a thermoelectric module is limited by the temperature-averaged figure of merit zT of both the n and p legs of the module [7–9], with

$$zT = \frac{\sigma S^2}{\kappa} T,$$

in which σ is the electrical conductivity, S is the Seebeck coefficient, and κ is the thermal conductivity, often dominated by phonons in doped semiconductors. The use of thermoelectric devices on a large scale would require a figure of merit of at least 2 to 3, depending on the application area [10,11]. The thermal averaging must be done between the temperature of the heat source and that of the heat sink, meaning that the materials composing the legs should have a good figure of merit in a wide range of temperatures. Additionally, the efficiency and reliability of the device are partly determined by the compatibility between the two legs, so ideally they should be made of similar compounds, such as a single semiconductor host with a different doping [10,12].

So far, most progress in boosting the thermoelectric figure of merit has been accomplished by lowering the thermal conductivity [13,14]. Enhancing the power factor (PF) σS^2 is a much more formidable challenge due to the interplay between the electrical conductivity and the Seebeck coefficient. To go beyond the rigid-band doping optimum, various band engineering strategies have been proposed, such as band convergence [15–17] and dimensional confinement of the electron gas [18–21]. Another promising method to boost the PF consists in using resonant states [22–24]. The concept is illustrated in Fig. 1. Dopants introduce impurity states inside the conduction band that hybridize with the extended states. This way, a sharp peak in the density of states (DOS) of the host compound is created, which alters the electronic transport properties when the Fermi level lies in its vicinity. An enhancement of the thermoelectric properties through resonant impurity states has been claimed in various compounds, such as Tl-doped PbTe [25], Sn-doped Bi_2Te_3 [26], In-doped SnTe [27], Al-doped PbSe [28], or Sn-doped β-As_2Te_3 [29]. The case of Tl-doped PbTe is controversial since first-principles calculations reproduced the experimental values for the Seebeck coefficient with a simple rigid-band shift of the pristine material [30]. Subsequently, numerical studies using the coherent potential approximation (CPA) coupled with first-principles calculations [31] have been conducted to investigate the effects of random Tl doping in PbTe [32–34]. However, transport properties were calculated in the absence of electron-phonon scattering, and the treatment of disorder by CPA methods is known to ignore the vertex corrections and thus localization effects [35]. More importantly, no clear improvement in the PF over a rigid-band shift of the Fermi level was shown for Tl-doped PbTe. As it stands, there is still no consensus in the literature whether actual resonant enhancement of the thermoelectric properties has been observed experimentally.

In this paper, we aim to clarify the general conditions required for a boost of the PF using resonant substitution impurities, all with a full treatment of the disorder and

*simon.thebaud@univ-lyon1.fr

 ©2019 American Physical Society

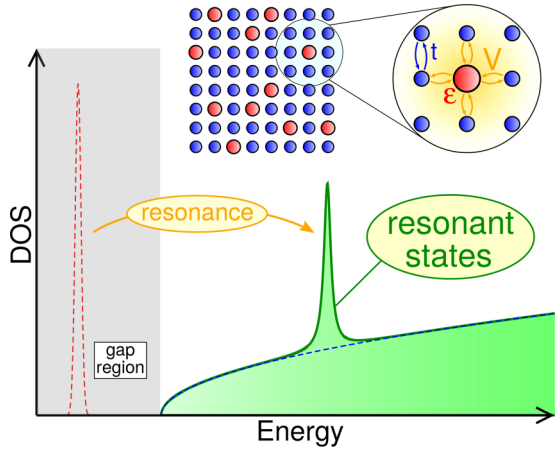

FIG. 1. Sketch of the density of states as a function of energy corresponding to a conduction band in the presence of resonant states. Inset: Illustration of the Hamiltonian terms.

resonant scattering. In particular, we will investigate the influence of the impurity concentration x and the effects of inelastic scattering, and finally we will examine the case of anisotropic orbitals.

II. DISORDERED MODEL HAMILTONIAN AND METHODOLOGY

To keep the conclusions as general as possible, we consider a single-orbital tight-binding Hamiltonian featuring hopping terms t between nearest neighbors on a cubic lattice. Here the charge carriers are electrons (n type), but because of electron-hole symmetry our results are valid for p-type materials as well. The resonant impurities are modeled by an on-site potential ϵ on the defect sites and a hybridization V between the host and impurity sites. The positions of the defects are chosen randomly. Hence, the Hamiltonian, as illustrated in the inset of Fig. 1, reads

$$\hat{H} = -t \sum_{\langle \mathbf{i},\mathbf{j}\rangle,\sigma} (c^{\dagger}_{\mathbf{i},\sigma} c_{\mathbf{j},\sigma} + c^{\dagger}_{\mathbf{j},\sigma} c_{\mathbf{i},\sigma}) + \epsilon \sum_{\mathbf{m},\sigma} c^{\dagger}_{\mathbf{m},\sigma} c_{\mathbf{m},\sigma} - V \sum_{\langle \mathbf{i},\mathbf{m}\rangle,\sigma} (c^{\dagger}_{\mathbf{i},\sigma} c_{\mathbf{m},\sigma} + c^{\dagger}_{\mathbf{m},\sigma} c_{\mathbf{i},\sigma}), \quad (1)$$

where $\mathbf{i}$ runs over host sites, $\mathbf{m}$ runs over impurity sites, σ is the electron spin, and the brackets denote nearest neighbors only. Since the transport properties do not depend explicitly on t, we express the other parameters in units of t (see below).

The electrical conductivity and the Seebeck coefficient at electron density n and temperature T are written [36,37]

$$\sigma(n,T) = \int dE \left(-\frac{\partial f}{\partial E}\right) \Sigma(E), \quad (2)$$

and

$$S(n,T) = -\frac{1}{eT\sigma} \int dE \left(-\frac{\partial f}{\partial E}\right) (E-\mu)\, \Sigma(E), \quad (3)$$

with $f(E,\mu,T)$ the Fermi distribution. The chemical potential μ is set to give the correct electron density when the DOS $\rho(E)$ is integrated. $\Sigma(E)$ is the so-called transport distribution function (TDF), which gives access to all the electronic transport properties and is therefore the key quantity to be calculated. σ is the thermal average of Σ around the Fermi level μ, while S is basically the logarithmic derivative of Σ around μ [38]. Therefore, high Seebeck coefficients arise from strong, sharp variations in the TDF (i.e., large values of $|\frac{d\Sigma}{dE}|$). Most theoretical studies of doped thermoelectric materials compute the TDF within the framework of the Boltzmann transport equation with the relaxation-time approximation [36]. They either consider impurity scattering to be negligible compared to electron-phonon scattering [39–43] or estimate the electron-impurity scattering rate by second-order perturbation theory, i.e., Fermi's "golden rule" (FGR), using a model description for the impurity scattering [44–46]. This is reasonable when the doping does not significantly alter the electronic structure and causes only weak electron-impurity scattering, as is the case of La- or Nb-doped $SrTiO_3$, for instance [47]. But the whole point of resonant states is that they distort the band structure of the host material and introduce strong scattering. Therefore, in this paper, we go beyond the semiclassical Boltzmann formalism to incorporate the full effects of disorder and multiple resonant scattering. We use the Kubo formula expressed in terms of the Green's function $\hat{G}$ of the system [48–51]

$$\Sigma(E) = \frac{\hbar e^2}{\pi \Omega} \langle \mathrm{Tr}[\mathrm{Im}\hat{G}(E)\, \hat{v}_x\, \mathrm{Im}\hat{G}(E)\, \hat{v}_x] \rangle, \quad (4)$$

where brackets denote disorder averaging, Ω is the total volume, $\hat{v}_x = \frac{it}{\hbar} \sum_{\langle \mathbf{i},\mathbf{j}\rangle,\sigma} (x_{\mathbf{i}} - x_{\mathbf{j}})(c^{\dagger}_{\mathbf{i},\sigma} c_{\mathbf{j},\sigma} - c^{\dagger}_{\mathbf{j},\sigma} c_{\mathbf{i},\sigma})$ is the velocity operator along the transport direction x, and the Green's function is written

$$\hat{G}(E) = \frac{1}{E - \hat{H} + i\frac{\gamma_{\mathrm{in}}}{2}}. \quad (5)$$

A constant imaginary part has been introduced in the denominator of $\hat{G}(E)$ to account for the presence of inelastic-scattering mechanisms in the system, such as electron-phonon (e-ph) or electron-electron (e-e) collisions. This will be further discussed below. Σ can be expressed in terms of the adimensioned TDF $\tilde{\Sigma}$, with $\Sigma = \frac{e^2}{a\hbar}\tilde{\Sigma}$, and likewise for the power factor $\mathrm{PF} = \frac{k_B^2}{a\hbar}\tilde{\mathrm{PF}}$. For definiteness, we set $a = 4$ Å, which gives the same volume per atom as in Si or PbTe, leading to $\frac{e^2}{a\hbar} = 6.08 \times 10^3$ S/cm and $\frac{k_B^2}{a\hbar} = 45.18\ \mu\mathrm{W\,cm^{-1}\,K^{-2}}$.

The exact diagonalization of the Hamiltonian (1) would drastically limit the system sizes that could be studied with a reasonable amount of memory and computational time. Therefore, a good alternative to compute $\Sigma(E)$ exactly, fully including vertex corrections, is the Chebyshev polynomial Green's-function method (CPGF) [52,53]. It is a real-space approach particularly suitable for addressing the physics in disordered systems. A brief overview of the method follows. The Green's function $\hat{G}(E)$ is expanded on the Chebyshev polynomials basis:

$$\hat{G}(\tilde{E}) = \sum_{n=0}^{\infty} g_n(\tilde{z}) T_n(\tilde{\hat{H}}), \quad (6)$$

where $\tilde{z} = \tilde{E} + i\tilde{\gamma}_{\mathrm{in}}/2$ with $\tilde{E}$ and $\tilde{\gamma}_{\mathrm{in}}/2$ rescaled in the energy interval $[-1, 1]$, $T_n(\tilde{\hat{H}})$ are the Chebyshev polynomials

calculated by the recursion relation $T_{n+1}(\tilde{H}) = 2\tilde{H}T_n(\tilde{H}) - T_{n-1}(\tilde{H})$, and $g_n(z)$ are known complex functions given by

$$g_n(z) = -i(2-\delta_{n,0})\frac{(z-i\sqrt{1-z^2})^n}{\sqrt{1-z^2}}. \quad (7)$$

Inserting Eq. (6) into Eq. (4) yields

$$\Sigma(\tilde{E}) = \frac{\hbar e^2}{\pi\Omega}\sum_{n,n'}\mu_{n,n'}\,\mathrm{Im}g_n(\tilde{z})\,\mathrm{Im}g_{n'}(\tilde{z}), \quad (8)$$

with

$$\mu_{n,n'} = \langle \mathrm{Tr}[T_n(\tilde{H})\,\tilde{v}_x\,T_{n'}(\tilde{H})\,\tilde{v}_x]\rangle. \quad (9)$$

The quantities $\mu_{n,n'}$ are called the moments and are calculated by iterative multiplications of the Hamiltonian matrix operator. Due to the superior convergence properties of the Chebyshev polynomials [54] and to the presence of the inelastic self-energy, only a finite number of terms in Eq. (6) need to be computed in order to obtain the exact Green's function of the system. Around 1800×1800 moments are sufficient for the TDF to fully converge. Periodic boundary conditions are used to reach the thermodynamic limit more easily. Here, we compute the TDF on systems of size $N = 1200 \times 200 \times 200$ (48×10^6 sites); this slab geometry allows faster convergence. The trace in Eq. (9) is evaluated efficiently by a stochastic method involving random vectors as described in Refs. [52,53]. When calculating the TDF for such a large system size, only a few random vectors and disorder configurations are necessary. We have checked that the clean limit is perfectly recovered for both open and periodic boundary conditions.

Regarding γ_{in} in Eq. (5), it can be interpreted as the inelastic contribution to the electron relaxation time [55]. In thermoelectric materials, scattering rates at room temperature typically range from 1 to 100 meV. In certain half Heuslers such as ZrNiSn, for instance, particularly weak *e*-ph couplings lead to inelastic-scattering rates varying between 1 and 20 meV [56] while strong *e*-*e* scattering in $SrTiO_3$ leads to γ_{in} ranging from 50 to 200 meV and even higher [47]. In between, scattering rates vary from 10 to 100 meV in Si [46,57,58] or from 20 to 60 meV in pristine and doped SnSe [59]. From the bandwidth in these compounds, we estimate t ranging from 0.3 to 1 eV, therefore we will consider $0.02\,t \leqslant \gamma_{\mathrm{in}} \leqslant 0.2\,t$. This corresponds to γ_{in} ranging from 10 to 200 meV and mean free paths between 50 Å and 500 Å in the pristine case, which is well in line with calculated values in PbTe [40], for instance. As we will see shortly, a small inelastic scattering is most favorable for resonant enhancements of the PF, therefore we set $\gamma_{\mathrm{in}} = 0.02\,t$ unless specified otherwise. The choice of a constant γ_{in} preserves the generality of this investigation, since incorporating energy and temperature dependences requires a material-specific study. Note also that computations for smaller γ_{in} would imply a strong increase in the number of calculated moments before convergence is reached.

III. NUMERICAL RESULTS AND DISCUSSION

In what follows, we consider the set of values $\epsilon = -4\,t$ and $V = 0.3\,t$ that were found optimal in a previous study that completely ignored disorder [60]. Unless specified otherwise, the electronic properties will be calculated using these values. Figure 2(a) shows the TDF and the DOS (inset) for different impurity concentrations $x = \frac{N_{\mathrm{imp}}}{N}$, with N_{imp} the number of randomly distributed defects. Five concentrations are considered, from $x = 0\%$ (the pristine reference case) to $x = 5\%$. The defects introduce a local peak in the DOS, which is considered the main signature of resonant states in the literature, and the mechanism by which the transport properties are enhanced. The higher the impurity concentration, the bigger and sharper the peak, so we would expect the best thermoelectric performances from the highest concentrations. As we will see shortly, this is not the case. The resonant peak gives rise in the TDF to a sharp, asymmetrical dip, as the extended states acquire a more localized character by hybridizing with impurity states. At high defect concentrations, electron transport is more suppressed across the whole energy range so the variations of the TDF are gentler ($|\frac{d\Sigma}{dE}|$ is reduced as x increases). We compare in Fig. 2(b) the TDF and $\frac{d\Sigma}{dE}$ calculated by CPGF and by the often used

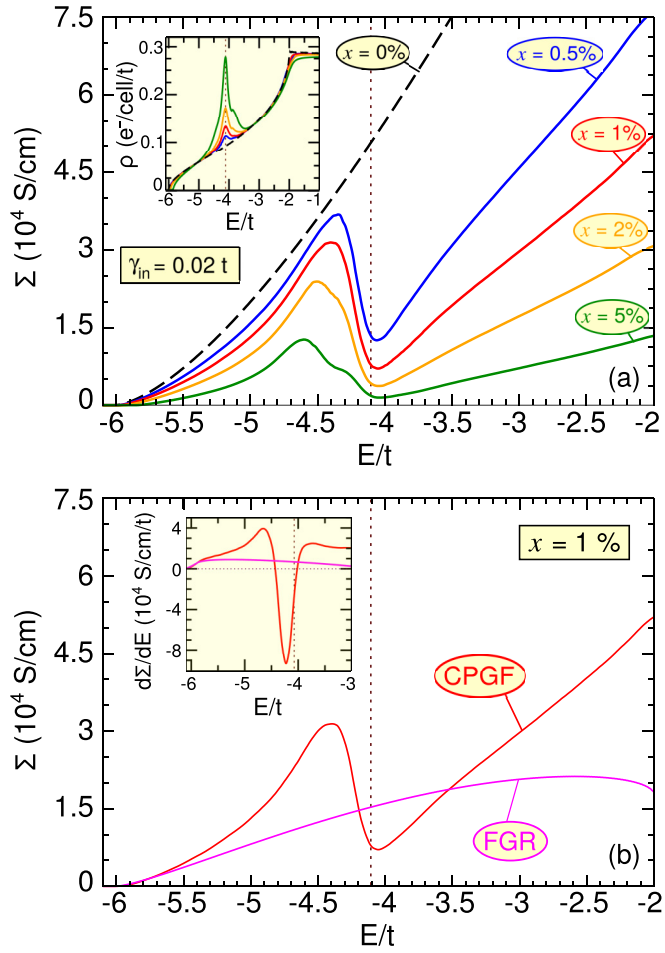

FIG. 2. (a) Transport distribution function $\Sigma(E)$ and density of states $\rho(E)$ (inset) for five impurity concentrations, from $x = 0\%$ (reference, black dashed line) to $x = 5\%$. A vertical dashed line marks the position of the resonant peak. (b) $\Sigma(E)$ and its derivative (inset) for $x = 1\%$ calculated exactly (CPGF) and by second-order perturbation theory (FGR).

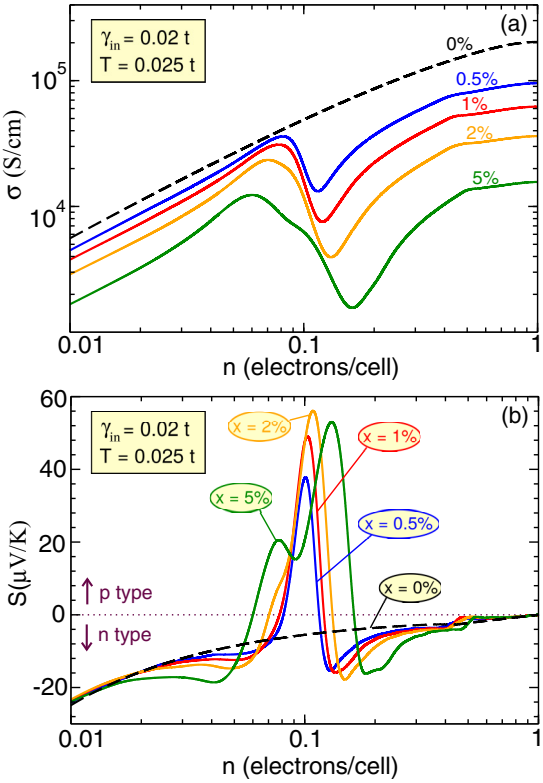

FIG. 3. (a) Electrical conductivity σ and (b) Seebeck coefficient S as a function of the electron density n for five impurity concentrations, from $x = 0$ to 5%.

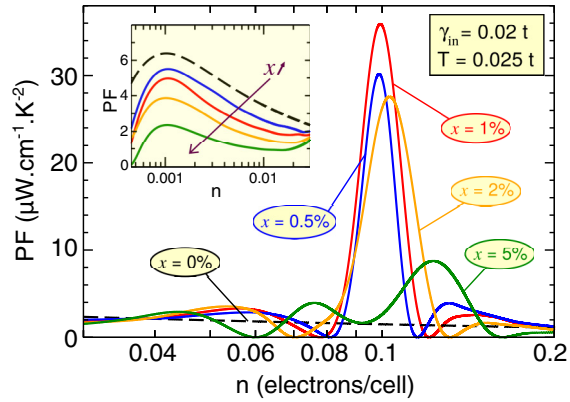

FIG. 4. Power factor σS^2 as a function of the electron density n for five impurity concentrations, from $x = 0$ to 5%. Inset: PF for lower electron densities.

FGR. Matthiessen's rule states that the total scattering rate is $\gamma_{tot} = \gamma_{imp} + \gamma_{in}$ with γ_{imp} the impurity scattering rate. FGR leads to $\gamma_{imp}(E) = 2\pi x\epsilon^2\rho_0(E)$, $\rho_0(E)$ being the DOS of the clean system. The FGR transport distribution function is given by $\Sigma_{FGR}(E) = \frac{\gamma_{in}}{\gamma_{tot}}\Sigma^{(0)}(E)$ where $\Sigma^{(0)}(E)$ is the pristine TDF. Notice that the exact $\Sigma(E)$ cannot be cast into such an analytical form. Clearly, the FGR approach completely fails to give the correct dependance of the TDF. In particular, the dip is entirely absent. The discrepancy is even worse for the derivatives, which are directly linked to the Seebeck coefficients. Therefore, when resonant states are involved, second-order perturbation theory breaks down.

From the results of Fig. 2(a) and Eqs. (2) and (3), we compute the room-temperature electrical conductivity σ and Seebeck coefficient S, as plotted in Fig. 3 as a function of the electron density n. T is set to $0.025\,t$, which corresponds to room temperature if $t \approx 1$ eV. σ is reduced by the disorder and still exhibits the same features as $\Sigma(E)$ (T being relatively small). This reduction would be detrimental to the PF, but the sharp variations in the TDF lead to a boost of the Seebeck coefficient that overcompensates the suppression of σ. This is accompanied by a sign inversion of S around $n = 0.1$ electrons/cell. Thus, S can change sign in the disordered systems, while it remains n type in the absence of resonant states. This interesting feature opens the possibility of changing the thermoelectric material from n type to p type just by introducing the appropriate impurity or dopant. Therefore, one could build a device with both n and p legs from the same semiconductor host. This would be advantageous for device performance and reliability, provided that the PF is sufficiently large.

The PF is plotted in Fig. 4 as a function of n. The pristine system exhibits a maximum of 6.3 μW cm^{-1} K^{-2} around $n = 10^{-3}$ electrons/cell, corresponding to a conductivity of 400 S/cm and a Seebeck coefficient of -130 μV/K. Note that this relatively low value of the power factor is partly due to the absence of band degeneracy and anisotropy in our single-band model. The effects of resonant impurities relative to the pristine case would not be affected by band degeneracy; the case of anisotropic orbitals will be examined below. When resonant defects are introduced, the PF is suppressed at low densities (inset), because multiple impurity scatterings have a stronger effect on the long-wavelength carriers. By contrast, around $n = 0.1$ electrons/cell, the PF now exhibits a large enhancement due to the boost of the Seebeck coefficient that overcompensates the drop in conductivity. The largest increase corresponds to $x = 1\%$, for which the PF reaches its maximum 35.9 μW cm^{-1} K^{-2}, a sixfold enhancement compared to that of the clean system. For $x = 5\%$, the boost is still present but less spectacular (a ratio less than 2) due to the gentler variations in the TDF. This is an important and surprising finding: to achieve an efficient enhancement of the thermoelectric properties with resonant states, the defect concentration should be kept relatively low, typically around 1%. From an experimental point of view, that is favorable, because such concentrations usually lie below the solubility limit [61]. Codoping with a donor atom acting as an electron reservoir is necessary to shift the Fermi level inside the resonant peak, where the PF is enhanced and the Seebeck inversion occurs. This carrier density optimization still requires at most 10% codoping, which is reasonable. We define PF_{max} as the optimum PF with respect to the carrier concentration. PF_{max} values extracted from Fig. 4 are shown in the first row of Table I.

We now address the influence of both ϵ and V on the transport properties. In Fig. 5(a), the DOS and TDF are plotted for $x = 1\%$ resonant impurities with $\epsilon = -5.5\,t$ and $V = 0.3\,t$. The increase of the on-site potential shifts the position of the resonant peak much closer to the bottom of the conduction band. The resulting TDF also features a much smaller dip

TABLE I. Room-temperature optimum power factor in μW cm^{-1} K^{-2} for $\gamma_{in} = 0.02\,t$ and several values of the on-site potential and hybridization parameter.

	$x = 0\%$	0.5%	1%	2%	5%
$\epsilon = -4\,t$ $V = 0.3\,t$	6.3	30.2	35.9	27.6	8.7
$\epsilon = -5.5\,t$ $V = 0.3\,t$	6.3	1.3	1.7	1.8	1.8
$\epsilon = -4\,t$ $V = t$	6.3	0.01	0.05	0.06	0.05

in $\Sigma(E)$ at the position of the peak in $\rho(E)$. Consequently, $|\frac{d\Sigma}{dE}|$ remains quite weak, and so does the Seebeck coefficient. There is still a sign inversion, but no boost in the PF. Indeed it is even suppressed by a factor 3–4 with respect to the reference value of 6.3 μW cm^{-1} K^{-2} (see the second row of Table I). Thus the resonant peak should not be too close to the band edge, but deep inside the conduction band. We now focus on the effect of a larger hybridization, which implies a stronger coupling between conduction and defect states. Results are depicted in Fig. 5(b). The increase in hybridization also pushes the resonant states at the very edge of the band, and severely suppresses the TDF below $-5\,t$ (notice the scale in the inset). There is still a small dip in $\Sigma(E)$ and a sign inversion of S, but because the carriers are now so localized

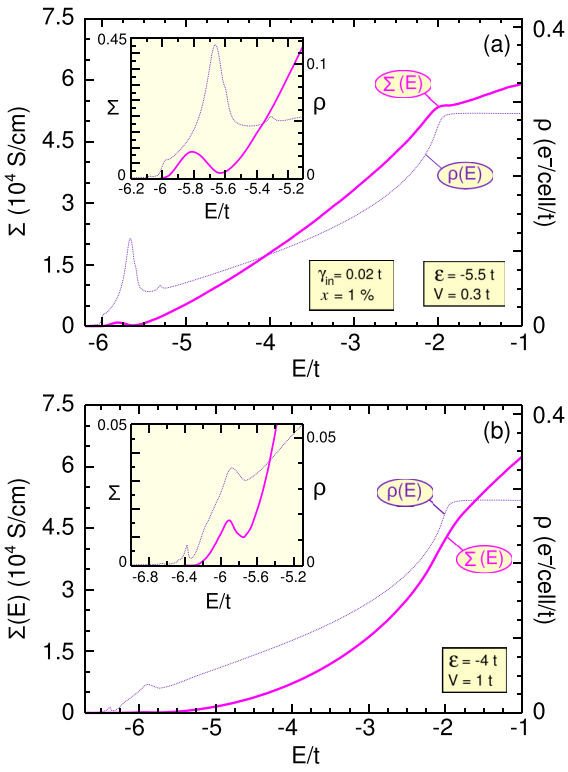

FIG. 5. Density of states $\rho(E)$ (dotted line, right axis) and transport distribution function $\Sigma(E)$ (left axis) for $x = 1\%$ with (a) $\epsilon = -5.5\,t$, $V = 0.3\,t$ and (b) $\epsilon = -4\,t$, $V = t$. Inset: Zoom on the bottom of the conduction band; notice the different scales for the TDF.

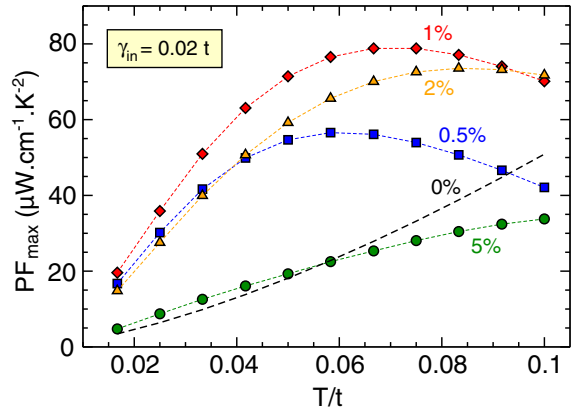

FIG. 6. Optimum power factor as a function of temperature for five impurity concentrations, from $x = 0$ to 5%.

in this energy range the PF shrinks by at least two orders of magnitude compared to that of the reference. For $x = 1\%$, PF_{max} is now 0.05 μW cm^{-1} K^{-2} (see the third row of Table I for the other concentrations). This suppression of the PF is entirely due to a huge reduction in the conductivity caused by multiple scattering events that become important at low energy in the presence of stronger disorder. These findings are consistent with the results obtained in Ref. [34] for Tl-doped PbTe, in which the Tl doping creates a resonant bump at the edge of the valence band associated with a much higher resistivity compared to that of Na doping, which behaves as a reservoir. It should also be mentioned that resonant states formed by antisites in Fe_2VAl have been found to suppress the PF by more than an order of magnitude while changing the sign of S [62]. The takeaway to obtain a boost of the PF is that the substituting element should be suitably selected in order to create a resonant peak far from the band edge. This could also explain why many claims of experimental enhancement of the PF by resonant states remain controversial, and why no sign inversion of the Seebeck coefficient has been observed so far. These effects are indeed sensitive to the hybridization, on-site potential, and position of the Fermi level. Additionally, it is difficult to rule out other enhancement mechanisms, such as energy filtering effects resulting from ionized impurity scattering, for instance.

Since thermoelectric materials are meant to be used in a wide range of temperature, we now discuss the T dependence of PF_{max}. Figure 6 shows PF_{max} as a function of temperature for the same impurity concentrations as in Fig. 4. It increases when the temperature rises, reaching a broad maximum, and then decreases slowly in the disordered systems. This high-temperature behavior results from the sharp variations in the TDF being smoothed out by the thermal average. Accordingly, at high values of x, the variations in the TDF are broader and are less sensitive to the thermal average, so the maximum region is shifted to higher temperatures. An important finding is that PF_{max} itself is robust, suggesting that resonant states could be efficient for both low- and high-temperature power generation.

We now propose to investigate the role of inelastic scattering. In Fig. 7(a), we plot PF_{max} as a function of γ_{in}. Clearly, the PF is completely suppressed if the inelastic scattering is too

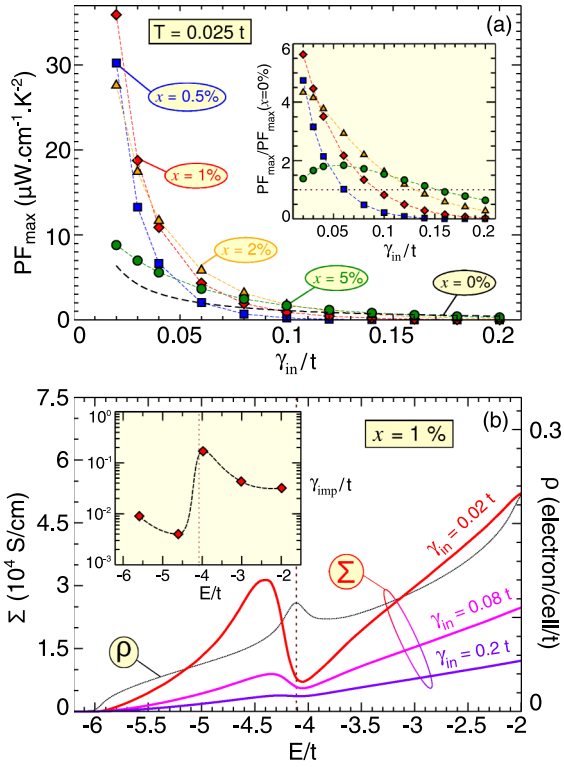

FIG. 7. (a) Optimum power factor as a function of the inelastic scattering rate γ_{in} for five impurity concentrations, from $x = 0$ to 5%. Inset: Ratio of the optimum power factor with respect to that of the clean system. (b) $\Sigma(E)$ for $x = 1\%$ with $\gamma_{\text{in}} = 0.02t$, $0.08t$, and $0.2t$ (left axis). $\rho(E)$ is also shown (dotted line, right axis). A vertical dashed line marks the position of the resonant peak. Inset: The calculated impurity scattering rate along the Γ-X direction as a function of energy. The dashed curve is a guide to the eye.

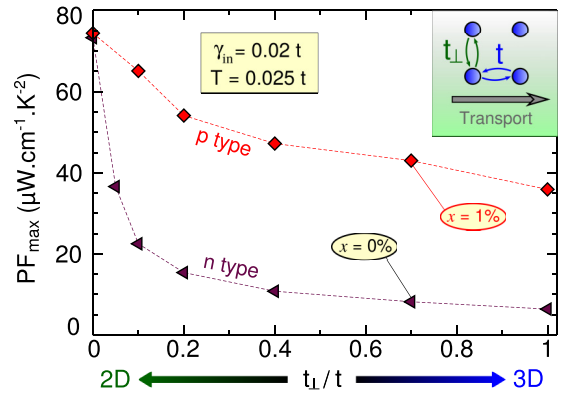

FIG. 8. Optimum power factor as a function of the anisotropy ratio $t_\perp/t$ for $x = 0\%$ (reference) and $x = 1\%$.

strong. This results from the competition between resonant impurity scatterings (elastic processes) and inelastic scatterings. In Fig. 7(b) is presented the TDF for $\gamma_{\text{in}} = 0.02t$, $0.08t$, and $0.2t$ with $x = 1\%$. The inset shows the impurity scattering rate γ_{imp}, extracted from an analysis of the single-particle spectral function $A(\mathbf{q}, E) = -\frac{1}{\pi}\langle \text{Im}G(\mathbf{q}, E)\rangle$. $G(\mathbf{q}, E)$ is the spatial Fourier transform of the disordered Green's function $G_{\mathbf{ij},\sigma}(E) = \langle \mathbf{i}\sigma|\hat{G}(E)|\mathbf{j}\sigma\rangle$, where $|\mathbf{i}\sigma\rangle$ is the real-space basis ($\mathbf{i}$ runs over the lattice sites). γ_{imp} exhibits a nonmonotonic behavior and large variations across the resonant peak, from $4 \times 10^{-3}\,t$ at $E = -4.5\,t$ to $2 \times 10^{-1}\,t$ at $-4\,t$. At the position of the dip in the TDF, where the electronic states have a stronger localized character, transport is not very sensitive to the strength of γ_{in} because $\gamma_{\text{imp}} \approx 2 \times 10^{-1}\,t$ dominates. In contrast, if γ_{imp} is smaller than γ_{in}, which is the case for states associated with large values of the TDF ($\gamma_{\text{imp}} \approx 4 \times 10^{-3}\,t$ at $E = -4.5\,t$), then increasing γ_{in} strongly suppresses $\Sigma(E)$. Thus, large inelastic-scattering rates have the overall effect of reducing the disparities in the TDF, leading to poor values of the Seebeck coefficient. If we now consider small values of γ_{in} (below $0.03\,t$) for $x \leqslant 2\%$, we observe a huge increase of PF_{max} as γ_{in} is reduced. If we extrapolate to $\gamma_{\text{in}} \leqslant 0.02\,t$ for $x = 1\%$, an enhancement factor of more than an order of magnitude could even be reached. Hence, due to the competition between elastic and inelastic scattering, the impurity concentration should be tuned with respect to the inelastic-scattering rate in the host material to reach an optimal boost of the PF. Compounds exhibiting strong *e*-ph or *e*-*e* scattering should not be the best candidates for resonant substitution doping.

Till now, we have been considering an isotropic electronic structure (*s*-type orbitals), but it is worth considering the influence of orbital anisotropy [63,64]. Low-dimensional confinement is expected to introduce sharp structures in the DOS and thus sharp variations in the TDF, thereby boosting the Seebeck coefficient. To evaluate the gain in the PF that could be obtained from resonant states in anistropic systems, we now introduce a different hopping $t_\perp$ in a direction perpendicular to transport. The optimum PF for the reference $x = 0\%$ and for $x = 1\%$ is presented in Fig. 8 as a function of $t_\perp/t$. First notice that the PF of the pristine system strongly increases with the anisotropy, from $6.3\,\mu\text{W cm}^{-1}\,\text{K}^{-2}$ (three dimensions) to $73.3\,\mu\text{W cm}^{-1}\,\text{K}^{-2}$ (two dimensions). This confirms that two-dimensional confinement in itself does favor good performances. The maximum PF (*p* type) for $x = 1\%$ also increases with the anisotropy, from $35.9\,\mu\text{W cm}^{-1}\,\text{K}^{-2}$ (three dimensions) to $74.4\,\mu\text{W cm}^{-1}\,\text{K}^{-2}$ (two dimensions). Surprisingly, for $t_\perp = 0$ we find no boost in the PF, suggesting that the presence of resonant states in fully confined systems might not further enhance the thermoelectric properties. However, one should emphasize that even for finite but low ratios $t_\perp/t$ (down to 0.05) the PF can be significantly increased by resonant states. This is promising for bulk systems in which charge carriers populate highly anisotropic orbitals. This is, for instance, the case of *n*-doped $SrTiO_3$, in which the titanium $3d$ orbitals exhibit a $t_\perp/t \approx 0.1$ [47,65]. Moreover, using resonant states in fully confined materials could be interesting for the sign inversion of S alone.

To conclude, we have used the Chebyshev polynomial Green's-function method to address the effects of resonant impurities on electron transport. Although resonant states suppress the electrical conductivity, they may also lead to a boost and a sign inversion of the Seebeck coefficient. Consequently, the power factor can increase by one order of magnitude. However, the resonant peak should be located far from the band edge, otherwise the thermoelectric performances are destroyed. Additionally, the optimal boost of the power factor depends crucially on the interplay between elastic and

inelastic scattering. Strong electron-phonon and electron-electron scatterings are found to preclude the possibility of enhancing thermoelectric transport. Therefore, materials featuring long electron mean free paths and weak inelastic scattering, such as PbTe [40], certain half-Heuslers compounds [56], or even graphene [66,67], should be promising candidates. Finally, the resonant boost of the power factor is found robust in the case of anisotropic orbitals. This paper will hopefully contribute to a better understanding of resonant states in the context of thermoelectric power generation. Our methodology is very general and can be combined with realistic first-principles calculations to guide experimentalists and pave the way in the search for compounds exhibiting resonant effects.

[1] C. Forman, I. K. Muritala, R. Pardemann, and B. Meyer, Renewable Sustainable Energy Rev. **57**, 1568 (2016).
[2] X. F. Zheng, C. X. Liu, and Q. Wang, Renewable and Sustainable Energy Rev. **32**, 486 (2011).
[3] M. H. Elsheikh, D. A. Shnawah, M. F. M. Sabri, S. B. M. Said, M. H. Hassan, M. B. A. Bashir, and M. Mohamad, Renewable and Sustainable Energy Rev. **30**, 337 (2014).
[4] X. Zhang and L.-D. Zhao, J. Materiomics **1**, 92 (2015).
[5] T. Zhu, Y. Liu, C. Fu, J. P. Heremans, J. G. Snyder, and X. Zhao, Adv. Mater. **29**, 1605884 (2017).
[6] G. D. Mahan, APL Mater. **4**, 104806 (2016).
[7] V. Zlatic and R. Monnier, *Modern Theory of Thermoelectricity* (Oxford University, New York, 2014).
[8] H. J. Goldsmid, *Introduction to Thermoelectricity* (Springer, New York, 2009).
[9] G. J. Snyder and T. S. Ursell, Phys. Rev. Lett. **91**, 148301 (2003).
[10] L. E. Bell, Science **321**, 1457 (2008).
[11] A. Thekdi and S. U. Nimbalkar, E3M Technical Report, 2015, doi:10.2172/1185778.
[12] R. He, G. Schierning, and K. Nielsch, Adv. Mater. Technologies **3**, 1700256 (2018).
[13] M. G. Kanatzidis, Chem. Mater. **22**, 648 (2010).
[14] G. J. Snyder and E. S. Toberer, Nat. Mater. **7**, 105 (2008).
[15] Y. Pei, H. Wang, and S. G. J., Adv. Mater. **24**, 6125 (2012).
[16] J. Yang, L. Xi, W. Qiu, L. Wu, X. Shi, L. Chen, J. Yang, W. Zhang, C. Uher, and D. J. Singh, npj Comput. Mater. **2**, 15015 (2015).
[17] Y. Pei, X. Shi, A. LaLonde, H. Wang, L. Chen, and G. J. Snyder, Nature (London) **473**, 66 (2011).
[18] L. D. Hicks and M. S. Dresselhaus, Phys. Rev. B **47**, 12727 (1993).
[19] J. P. Heremans, Acta Phys. Polon. A **108**, 609 (2005), Proceedings of the XXXIV International School of Semiconducting Compounds.
[20] M. S. Dresselhaus, G. Chen, M. Y. Tang, R. G. Yang, H. Lee, D. Z. Wang, Z. F. Ren, J.-P. Fleurial, and P. Gogna, Adv. Mater. **19**, 1043 (2007).
[21] P. Pichanusakorn and B. Prabhakar, Mater. Sci. Eng. R **67**, 19 (2010).
[22] J. P. Heremans, B. Wiendlocha, and A. M. Chamoire, Energy Environ. Sci. **5**, 5510 (2012).
[23] G. D. Mahan and J. O. Sofo, Proc. Natl. Acad. Sci. USA **93**, 7436 (1996).
[24] J. Zhou, R. Yang, G. Chen, and M. S. Dresselhaus, Phys. Rev. Lett. **107**, 226601 (2011).
[25] J. P. Heremans, V. Jovovic, E. S. Toberer, A. Saramat, K. Kurosaki, A. Charoenphakdee, S. Yamanaka, and G. J. Snyder, Science **321**, 554 (2008).
[26] C. M. Jaworski, V. Kulbachinskii, and J. P. Heremans, Phys. Rev. B **80**, 233201 (2009).
[27] Q. Zhang, B. Liao, Y. Lan, K. Lukas, W. Liu, K. Esfarjani, C. Opeil, D. Broido, G. Chen, and Z. Ren, PNAS **110**, 13261 (2013).
[28] Q. Zhang, H. Wang, W. Liu, H. Wang, B. Yu, Q. Zhang, Z. Tian, G. Ni, S. Lee, K. Esfarjani *et al.*, Energy Environ. Sci. **5**, 5246 (2012).
[29] B. Wiendlocha, J.-B. Vaney, C. Candolfi, A. Dauscher, B. Lenoir, and J. Tobola, Phys. Chem. Chem. Phys. **20**, 12948 (2018).
[30] D. J. Singh, Phys. Rev. B **81**, 195217 (2010).
[31] H. Ebert, D. Ködderitzsch, and J. Minár, J. Rep. Prog. Phys. **74**, 096501 (2011).
[32] B. Wiendlocha, K. Kutorasinski, S. Kaprzyk, and J. Tobola, Scr. Mater. **111**, 33 (2016).
[33] B. Wiendlocha, Phys. Rev. B **88**, 205205 (2013).
[34] B. Wiendlocha, Phys. Rev. B **97**, 205203 (2018).
[35] E. N. Economou, *Green's Functions in Quantum Physics* (Springer, New York, 1979).
[36] N. W. Ashcroft and N. D. Mermin, *Solid State Physics* (Saunders, Philadelphia, 1976).
[37] T. J. Scheidemantel, C. Ambrosch-Draxl, T. Thonhauser, J. V. Badding, and J. O. Sofo, Phys. Rev. B **68**, 125210 (2003).
[38] M. Cutler and N. F. Mott, Phys. Rev. **181**, 1336 (1969).
[39] J. Sun and D. J. Singh, J. Mater. Chem. A **5**, 8499 (2017).
[40] Q. Song, T.-H. Liu, J. Zhou, Z. Ding, and G. Chen, Mater. Today Phys. **2**, 69 (2017).
[41] D. Parker and D. J. Singh, Phys. Rev. B **82**, 035204 (2010).
[42] H. Peng, J.-H. Song, M. G. Kanatzidis, and A. J. Freeman, Phys. Rev. B **84**, 125207 (2011).
[43] X. H. Yang, X. Y. Qin, D. Li, J. Zhang, C. J. Song, Y. F. Liu, L. Wang, and H. X. Xin, J. Phys. Chem. Solids **86**, 74 (2015).
[44] Z. Wang, S. Wang, S. Obukhov, N. Vast, J. Sjakste, V. Tyuterev, and N. Mingo, Phys. Rev. B **83**, 205208 (2011).
[45] M. Zebarjadi, K. Esfarjani, M. S. Dresselhaus, Z. F. Ren, and G. Chen, Energy Environ. Sci. **5**, 5147 (2012).
[46] B. Qiu, Z. Tian, A. Vallabhaneni, B. Liao, J. M. Mendoza, O. D. Restrepo, X. Ruan, and G. Chen, Europhys. Lett. **109**, 57006 (2015).
[47] G. Bouzerar, S. Thébaud, C. Adessi, R. Debord, M. Apreutesei, R. Bachelet, and S. Pailhès, Europhys. Lett. **118**, 67004 (2017).
[48] D. A. Greenwood, Proc. Phys. Soc. **71**, 585 (1958).
[49] A. D. Stone and A. Szafer, IBM J. Res. Dev. **32**, 384 (1988).
[50] H. U. Baranger and A. D. Stone, Phys. Rev. B **40**, 8169 (1989).
[51] B. K. Nikolić, Phys. Rev. B **64**, 165303 (2001).
[52] A. Ferreira and E. R. Mucciolo, Phys. Rev. Lett. **115**, 106601 (2015).

[53] A. Weiße, G. Wellein, A. Alvermann, and H. Fehske, Rev. Mod. Phys. **78**, 275 (2006).
[54] J. P. Boyd, *Chebyshev and Fourier Spectral Methods*, Dover Books on Mathematics, 2nd ed. (Dover, New York, 2001).
[55] G. D. Mahan, *Many Particle Physics*, 3rd ed. (Plenum, New York, 2000).
[56] J. Zhou, H. Zhu, T.-H. Liu, Q. Song, R. He, J. Mao, Z. Liu, W. Ren, B. Liao, D. J. Singh *et al.*, Nat. Commun. **9**, 1721 (2018).
[57] E. Witkoske, X. Wang, M. Lundstrom, V. Askarpour, and J. Maassen, J. Appl. Phys. **122**, 175102 (2017).
[58] L. J. Zhang, P. Qin, C. Han, J. L. Wang, Z. H. Ge, Q. Sun, Z. X. Cheng, Z. Li, and S. X. Dou, J. Mater. Chem. A **6**, 2507 (2018).
[59] J. J. Meléndez and R. L. González-Romero, J. Alloys Compd. **757**, 70 (2018).
[60] S. Thébaud, C. Adessi, S. Pailhès, and G. Bouzerar, Phys. Rev. B **96**, 075201 (2017).
[61] V. E. Boeisenko and S. G. Yudin, Phys. Status Solidi A **101**, 123 (1987).
[62] D. I. Bilc and P. Ghosez, Phys. Rev. B **83**, 205204 (2011).
[63] D. Parker, X. Chen, and D. J. Singh, Phys. Rev. Lett. **110**, 146601 (2013).
[64] D. I. Bilc, G. Hautier, D. Waroquiers, G.-M. Rignanese, and P. Ghosez, Phys. Rev. Lett. **114**, 136601 (2015).
[65] Z. Zhong, P. Wissgott, K. Held, and G. Sangiovanni, Europhys. Lett. **99**, 37011 (2012).
[66] S. V. Morozov, K. S. Novoselov, M. I. Katsnelson, F. Schedin, D. C. Elias, J. A. Jaszczak, and A. K. Geim, Phys. Rev. Lett. **100**, 016602 (2008).
[67] A. H. Castro Neto, F. Guinea, N. M. R. Peres, K. S. Novoselov, and A. K. Geim, Rev. Mod. Phys. **81**, 109 (2009).